



ARTICLE

Frequency Adaptive Grid Synchronization Detection Algorithm Based on SOGI

Jie Shao¹, Zihao Zhang¹, Quan Xu¹, Tiantian Cai¹, Junye Li¹, Baicheng Xiang¹, Shijie Li¹ and Xianfeng Xu^{2,*}

¹China Southern Power Grid Co., Ltd., Guangzhou, 510663, China

²School of Energy and Electrical Engineering, Chang'an University, Xi'an, 710064, China

*Corresponding Author: Xianfeng Xu. Email: xxf@chd.edu.cn

Received: 10 January 2025; Accepted: 14 April 2025; Published: 29 May 2025

ABSTRACT: In response to the complex working conditions of the power grid caused by the high proportion of new energy access, which leads to insufficient output accuracy of the second-order generalized integrator (SOGI) phase-locked loop, this article proposes an improved frequency adaptive phase-locked loop structure for SOGI. Firstly, an amplitude compensation branch is introduced to compensate for the SOGI tracking fundamental frequency signal, ensuring the accuracy of the SOGI output orthogonal signal under frequency fluctuation conditions. Secondly, by cascading two adaptive SOGI modules, the suppression capability of low-order harmonics and Direct Current (DC) components has been improved. Finally, the positive and negative sequence separation method of orthogonal signals is introduced to eliminate the influence of unbalanced components on the phase-locked loop. The comparative experiment with the classic SOGI-PLL method shows that the proposed phase-locked loop structure effectively improves the accuracy of power grid synchronization detection under complex working conditions such as harmonic components, unbalanced components, and frequency fluctuations. It can complete frequency detection within 1.5 power frequency cycles, and the detected fundamental frequency positive sequence voltage has a higher sinusoid and harmonic distortion rate within 0.5%.

KEYWORDS: Phase-locked loop; second-order generalized integrator; pre-filtering; frequency adaptation; harmonic distortion

1 Introduction

With the expansion of renewable energy, the application of grid-connected inverters in the power system continues to increase [1]. As a key interface connecting distributed power sources and the power grid, precise control of the injected current into the grid can achieve grid synchronization support and power quality management, ensuring the stability and safety of the power system [2–5]. The implementation of high-quality synchronous grid-current injection for grid-connected inverters requires proper grid synchronization algorithms [6].

The existing grid synchronization algorithms are mainly based on PLL technology, which can effectively track changes in grid voltage [7,8]. However, due to the intermittency of renewable energy and the nonlinearity of power electronic devices, different operating conditions such as unbalanced components, harmonic distortion, and frequency fluctuations occur in the system [9,10]. Therefore, it is crucial to improve the steady-state accuracy and dynamic response performance of PLL under different operating conditions.



In order to improve performance under complex power grid conditions, researchers have proposed improvement measures applicable to different working conditions by enhancing the filtering ability of phase-locked loops, mainly including loop filtering and pre-filtering methods [11,12]. The loop filter will affect the adjustment of PLL parameters, resulting in poor stability and tracking speed [13], while the pre-filter faces the filtering problem of multiphase grid voltage [14]. Integrating delay filtering methods such as Moving Average Filter (MAF) and Delay Single Cancellation (DSC) in Synchronous Rotating Frame-PLL (SRF-PLL) [15–17] can be applied to pre-filtering and loop filtering, effectively reducing the impact of specific frequency grid harmonics and achieving better filtering capabilities, thereby obtaining more accurate grid voltage synchronization signals. In terms of frequency adaptive detection, by concatenating multiple filters with the same parameters and increasing the width of the notch frequency band, it is possible to achieve adaptive detection of small frequency fluctuations [18]; There are also studies that use negative feedback to compensate for amplitude and phase angle errors, achieving wideband frequency adaptive detection [19]. However, the above two filtering methods are cumbersome in parameter design for complex harmonic signals, and when the frequency of power grid harmonics changes, the overall filtering structure needs to be redesigned, which is not universal. A notch filter (NF) similar to delay filtering can also selectively eliminate harmonic components [20], however, multiple NFs need to be cascaded in the PLL control loop, which increases the complexity of the PLL structure. Reference [21] proposed a structurally simple complex coefficient filtering phase-locked loop (CCF-PLL), which can achieve fast and accurate phase locking under unbalanced power grid voltage. However, the bandpass filtering performance limits the filtering effect, and the detection phase and frequency errors are relatively large.

The classic generalized integrator structure is widely used in pre-filtering, and its output orthogonal signal features can stably extract the positive and negative sequence components of the grid voltage, with good steady-state and transient performance. Reference [22] proposed a Sine amplitude integrator phase-locked loop (SAI-PLL), which uses two cross decoupled sine amplitude integrators to separate the positive and negative sequence components of the grid voltage. It also introduces a frequency adaptive unit, which can effectively detect the frequency and phase of the grid voltage when the three-phase voltage is unbalanced and there is a frequency step. Reference [23] proposes a phase-locked loop structure based on the SOGI, which has better filtering performance than SAI-PLL, but cannot eliminate the influence of DC components. Reference [24] proposes adding a filtering element to the second-order generalized integrator to form a third-order generalized integrator phase-locked loop (TOGI-PLL), which can further suppress the influence of DC components. However, due to the limitation of the frequency selection characteristics of the generalized integrator, the filtering effect on low-order harmonics is poor, and the low-order harmonic content in the power grid is often high, which has a significant impact on the accuracy of the phase-locked loop. And frequency fluctuations will cause errors in the output fundamental wave. In addition, researchers have combined the different filters mentioned above to leverage their optimal characteristics and applied them separately to in-loop filtering and pre-filtering, achieving a hybrid filtering phase-locked loop structure [25]. However, the design structure of hybrid filtering is relatively complex and may also have significant delays.

This article optimizes the SOGI structure in terms of frequency adaptation and filtering, based on its superior filtering and output performance. By analyzing the characteristics of SOGI output under frequency fluctuations, an amplitude compensation branch was designed to eliminate errors, ensuring the stability and accuracy of tracking the fundamental frequency grid signal under different frequency conditions; Aiming at the problem of SOGI lacking DC component and insufficient filtering ability, a cascaded structure of two adaptive SOGI was designed for optimization, and the resulting cascaded structure has better filtering ability and DC bias suppression ability; Furthermore, for the orthogonal signals output by SOGI, a positive-negative sequence separation method is introduced to achieve the separation of positive and negative sequence

voltages in unbalanced power grids. Finally, the optimized structure designed should be included in the PLL pre-filtering stage to achieve grid synchronization detection function. Through two experiments, it was verified that the designed phase-locked loop structure could stably detect power grid information under frequency fluctuations, harmonic disturbances, and unbalanced component disturbances. Compared with SOGI-PLL, the designed structure has higher accuracy and faster dynamic response speed.

2 SOGI Pre-Filter Phase-Locked Loop Structure

This section mainly discusses the structure of the phase-locked loop and the SOGI pre-filtering method.

2.1 SRF-PLL Structure

The structure of the phase-locked loop with pre-filtering is shown in Fig. 1.

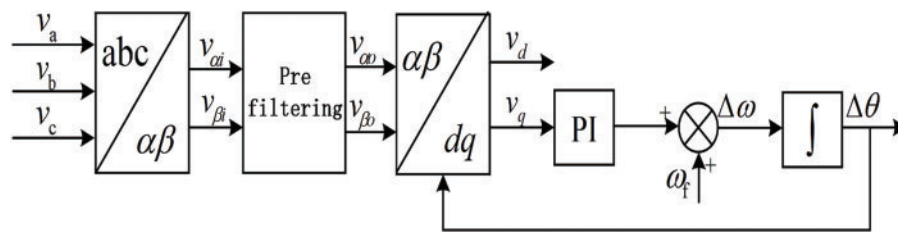


Figure 1: Structure diagram of SRF-PLL for pre-filtering

SRF-PLL converts the three-phase voltage signals (v_a, v_b, v_c) into two-phase orthogonal signals ($v_{\alpha i}$ and $v_{\beta i}$) through Clark transform, as shown in Eq. (1).

$$\begin{bmatrix} v_{\alpha} \\ v_{\beta} \end{bmatrix} = \frac{2}{3} \begin{bmatrix} 1 & -\frac{1}{2} & -\frac{1}{2} \\ 0 & \frac{\sqrt{3}}{2} & -\frac{\sqrt{3}}{2} \end{bmatrix} \begin{bmatrix} v_a \\ v_b \\ v_c \end{bmatrix} = v \begin{bmatrix} \cos \varphi \\ \sin \varphi \end{bmatrix}. \quad (1)$$

By eliminating the disturbance components in the power grid through pre-filtering, the fundamental frequency orthogonal signals $v_{\alpha o}$ and $v_{\beta o}$ of the power grid are obtained, which are then transformed into v_d and v_q through Park transform, as shown in Eq. (2).

$$\begin{bmatrix} v_d \\ v_q \end{bmatrix} = \begin{bmatrix} \cos \theta & \sin \theta \\ -\sin \theta & \cos \theta \end{bmatrix} \begin{bmatrix} v_{\alpha} \\ v_{\beta} \end{bmatrix} = v \begin{bmatrix} \cos(\theta_g - \theta) \\ \sin(\theta_g - \theta) \end{bmatrix} \approx v \begin{bmatrix} 1 \\ \Delta \theta \end{bmatrix}. \quad (2)$$

Among them, θ_g is the phase of the three-phase power grid voltage, θ is the estimated output phase value of SRF-PLL, and $\Delta \theta$ is the phase error. According to Eq. (2), v_d is the amplitude estimation of the three-phase signal, and the v_q signal containing phase error information outputs a phase estimation error of $\Delta \omega_g$ through a PI controller, further completing the phase estimation and achieving the output of power grid frequency and phase.

2.2 SOGI Pre-Filtering Method

SOGI is a bandpass filter, which can track the fundamental signal and eliminate high-order harmonics in the pre-filtering stage. Its structure is shown in Fig. 2. In Fig. 2, v_i is the input grid voltage, v_o and qv_o are the two output signals of SOGI, with equal amplitudes and a phase difference of 90° . k is the damping coefficient

of SOGI, and ω_n is the resonant frequency of SOGI, which is used to determine the selection frequency of the signal. The value is usually set as the fundamental angular frequency of the grid, which is 100π .

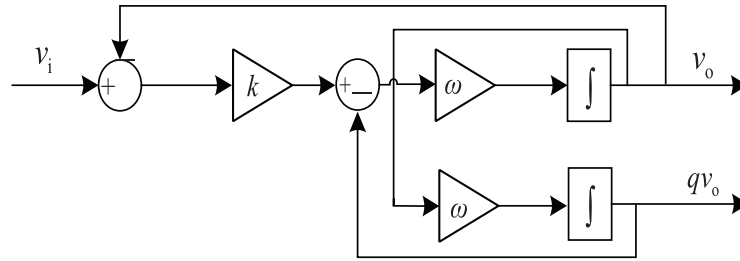


Figure 2: SOGI structure diagram

As shown in Fig. 2, the transfer function of SOGI [1,2]:

$$D_{\text{SOGI}}(s) = \frac{v_o(s)}{v_i(s)} = \frac{k\omega_n s}{s^2 + k\omega_n s + \omega_n^2}, \quad (3)$$

$$Q_{\text{SOGI}}(s) = \frac{qv_o(s)}{v_i(s)} = \frac{k\omega_n^2}{s^2 + k\omega_n s + \omega_n^2}. \quad (4)$$

The value of coefficient k determines the dynamic response capability and filtering capability of SOGI. Fig. 3 shows the Bode plots for $D_{\text{SOGI}}(s)$ and $Q_{\text{SOGI}}(s)$, respectively. As shown in the figure, the increase of k value weakens the filtering ability; On the contrary, as k decreases, the filtering ability improves, but the dynamic response speed slows down. Meanwhile, $Q_{\text{SOGI}}(s)$ exhibits low-pass filtering characteristics and has almost no filtering ability for signals with angular frequencies less than ω_n , which will result in a significant impact of DC components on signal extraction.

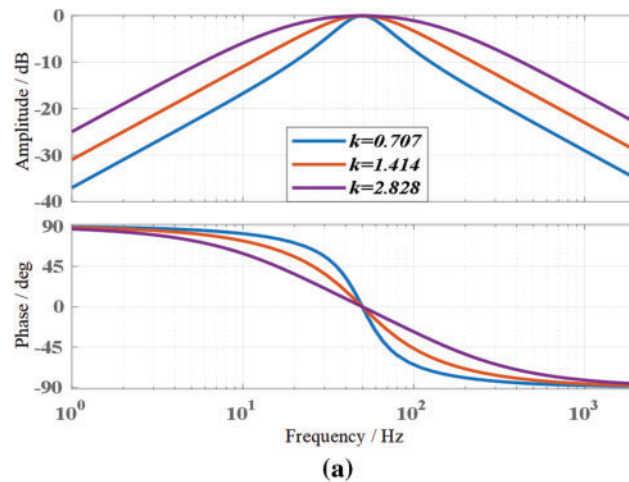


Figure 3: (Continued)

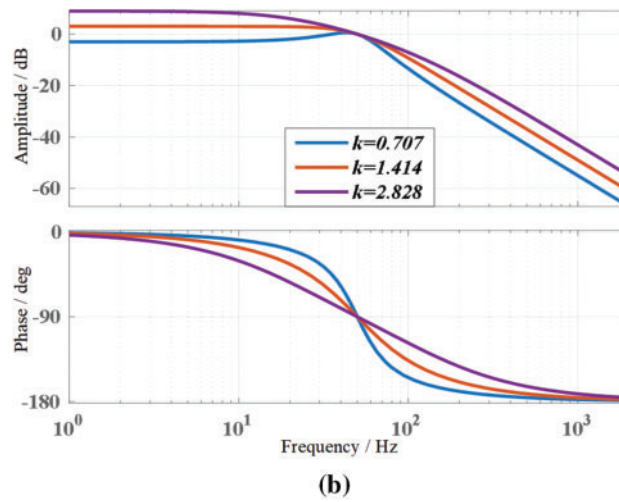


Figure 3: Bode plot of SOGI under different coefficients. (a) $D_{\text{SOGI}}(s)$ bode plot; (b) $Q_{\text{SOGI}}(s)$ bode plot

From the Bode plot of SOGI, it can be seen that when the frequency fluctuates, the fundamental frequency grid voltage signal tracked by SOGI output will experience amplitude attenuation. And SOGI has weak filtering ability for low-order harmonics. When the frequency decreases, the frequency points of each harmonic shift to the left, which will further weaken the filtering ability of low-order and low-order harmonics. Ultimately, it will have an impact on the accuracy of grid synchronization detection.

3 Improved SOGI Pre-Filter Phase-Locked Loop Structure

This section is based on the classic SOGI and designs suitable structures in terms of frequency adaptation and filtering capabilities.

3.1 Optimization of SOGI Frequency Adaptation

Assuming the grid voltage $v_i(t) = v \sin(\omega_g t)$, where v is the amplitude of the grid voltage and ω_g is the angular frequency of the grid voltage. After the voltage is filtered by SOGI, corresponding transformations are performed according to Eqs. (3) and (4) to obtain the expression of the output orthogonal signal in the time domain

$$v_o(t) = \frac{k\omega_n\omega_g}{\sqrt{k^2\omega_n^2\omega_g^2 + (\omega_n^2 - \omega_g^2)^2}} \sin(\omega_g t - \delta) - A \sin\left(\sqrt{1 - k^2/4}\omega_n t - \phi\right) e^{\frac{-k\omega_n t}{2}}, \quad (5)$$

$$v_{qo}(t) = \frac{-k\omega_n^2}{\sqrt{k^2\omega_n^2\omega_g^2 + (\omega_n^2 - \omega_g^2)^2}} \cos(\omega_g t - \delta) - A \sin\left(\sqrt{1 - k^2/4}\omega_n t - \phi\right) e^{\frac{-k\omega_n t}{2}}, \quad (6)$$

$$\sin(\delta) = \frac{\omega_g^2 - \omega_n^2}{\sqrt{k^2\omega_n^2\omega_g^2 + (\omega_n^2 - \omega_g^2)^2}}. \quad (7)$$

In Eqs. (5) and (6), parameters A and ϕ only affect the amplitude and phase angle of oscillations. This term decays exponentially with time t , and the time constant is small. This term will quickly decay to 0, without affecting the steady-state results of the system. The error angle generated by the frequency variation of the power grid is δ , as shown in Eq. (7). According to Eqs. (5)–(7), it can be seen that when the frequency

fluctuates, i.e., $\omega_n \neq \omega_g$, the orthogonal signal output by SOGI will produce amplitude and phase angle errors, which will affect the accuracy of grid synchronization detection.

When the system is in steady state, the voltage of the power grid on the $\alpha\beta$ axis, $v_{\alpha i}$ and $v_{\beta i}$, passes through the SOGI module and outputs $v_{\alpha o}$ and $v_{\beta o}$ through $D_{\text{SOGI}}(s)$, $v_{q\alpha o}$ and $v_{q\beta o}$ through $Q_{\text{SOGI}}(s)$. According to the transfer functions of Eqs. (3) and (4), the input-output relationship of the orthogonal signal is shown in the following equation

$$v_{\alpha o} = \frac{jk\omega_n\omega_g}{-\omega_g^2 + jk\omega_n\omega_g + \omega_n^2} v_{\alpha i}, \quad (8)$$

$$v_{q\alpha o} = \frac{k\omega_n^2}{-\omega_g^2 + jk\omega_n\omega_g + \omega_n^2} v_{\alpha i}, \quad (9)$$

$$v_{\beta o} = \frac{jk\omega_n\omega_g}{-\omega_g^2 + jk\omega_n\omega_g + \omega_n^2} v_{\beta i}, \quad (10)$$

$$v_{q\beta o} = \frac{k\omega_n^2}{-\omega_g^2 + jk\omega_n\omega_g + \omega_n^2} v_{\beta i}. \quad (11)$$

Convert the above four equations into input and output representations:

$$jv_{\alpha i} = \frac{(\omega_n^2 - \omega_g^2)}{k\omega_n\omega_g} (\omega_n^2 - \omega_g^2) v_{\alpha o} + jv_{\alpha o}, \quad (12)$$

$$v_{\alpha i} = \frac{\omega_g}{\omega_n} jv_{q\alpha o} + \frac{\omega_n^2 - \omega_g^2}{k\omega_n^2} v_{q\alpha o}, \quad (13)$$

$$jv_{\beta i} = \frac{(\omega_n^2 - \omega_g^2)}{k\omega_n\omega_g} (\omega_n^2 - \omega_g^2) v_{\beta o} + jv_{\beta o}, \quad (14)$$

$$v_{\beta i} = \frac{\omega_g}{\omega_n} jv_{q\beta o} + \frac{\omega_n^2 - \omega_g^2}{k\omega_n^2} v_{q\beta o}. \quad (15)$$

If $\omega_n = \omega_g$, the output results of the above four equations are $v_{\alpha i} = v_{\alpha o}$, $v_{q\alpha i} = v_{q\alpha o}$, $v_{\beta i} = v_{\beta o}$ and $v_{q\beta i} = v_{q\beta o}$. When $\omega_n \neq \omega_g$, there is an error term in the relationship between the above four inputs and outputs, let $v_{\alpha}^* = v_{\alpha i}$, $v_{q\alpha}^* = v_{q\alpha i}$, $v_{\beta}^* = v_{\beta i}$ and $v_{q\beta}^* = v_{q\beta i}$, where v_{α}^* , $v_{q\alpha}^*$, v_{β}^* and $v_{q\beta}^*$ are the new outputs corresponding to the input SOGI under frequency fluctuations. Meanwhile, by utilizing the relationship between orthogonal signals and substituting $v_{\alpha i} = jv_{\beta i}$ and $v_{\alpha o} = jv_{\beta o}$ into the above equation, the expression for the output orthogonal signal can be obtained:

$$v_{\alpha o}^* = v_{\alpha o} + \frac{\omega_n^2 - \omega_g^2}{k\omega_n\omega_g} v_{\beta o}, \quad (16)$$

$$v_{q\alpha o}^* = \frac{\omega_g}{\omega_n} v_{q\alpha o} + \frac{\omega_n^2 - \omega_g^2}{k\omega_n^2} v_{\beta o}, \quad (17)$$

$$v_{\beta o}^* = v_{\beta o} - \frac{\omega_n^2 - \omega_g^2}{k\omega_n\omega_g} v_{\alpha o}, \quad (18)$$

$$v_{q\beta o}^* = \frac{\omega_g}{\omega_n} v_{q\beta o} - \frac{\omega_n^2 - \omega_g^2}{k\omega_n^2} v_{\alpha o}. \quad (19)$$

According to Eqs. (16)–(19), frequency fluctuations will cause error terms in the output of the original SOGI, and the error term can be calculated from the orthogonal signal corresponding to that channel. Therefore, based on the orthogonal signal output by SOGI, a frequency adaptive amplitude compensation branch is constructed, and the corresponding frequency adaptive SOGI (FSOGI) structure is shown in Fig. 4.

In Fig. 4, k_1 , k_2 and k_3 correspond to three error coefficients, which are obtained through digital operations using fixed ω_n and grid angular frequency ω_g . By introducing an amplitude compensation branch and real-time feedback of the grid angular frequency to various coefficients, the accuracy of the fixed parameter ω_n pre-filter SOGI tracking the fundamental signal can be improved under frequency fluctuation conditions, thereby ensuring the accuracy of detecting the fundamental component of the grid.

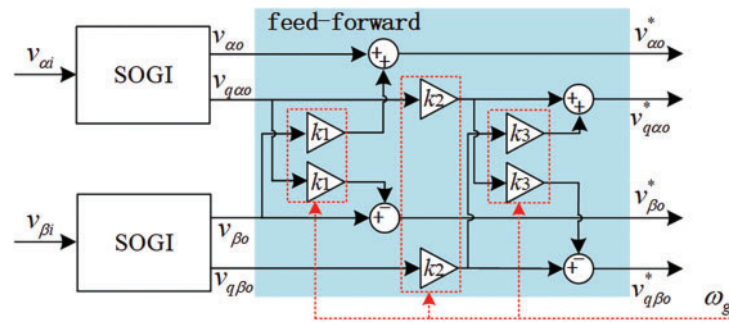


Figure 4: FSOGI frequency adaptive feedforward compensation structure

3.2 Optimization of SOGI Filtering Performance

In order to optimize the problem that SOGI cannot eliminate DC components and has weak filtering ability, two FSOGIs are metered to form Frequency Cascade SOGI (FCSOGI), and the channel with equal amplitude and phase angle output from FSOGI is used as the input of the next stage FSOGI. The overall structure is shown in Fig. 5.

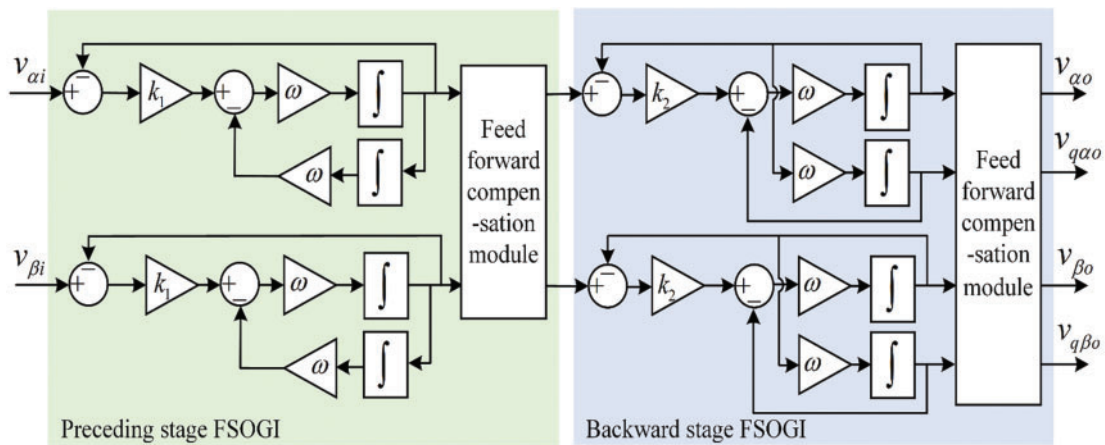


Figure 5: FCSOGI structure diagram

The constructed FCSOGI has two adjustable proportional parameters, which can provide a wider range of adjustments for filtering ability and dynamic response-ability. By adjusting and selecting the dynamic response and filtering capabilities of FCSOGI, the Bode plots under different parameters are shown in Fig. 6.

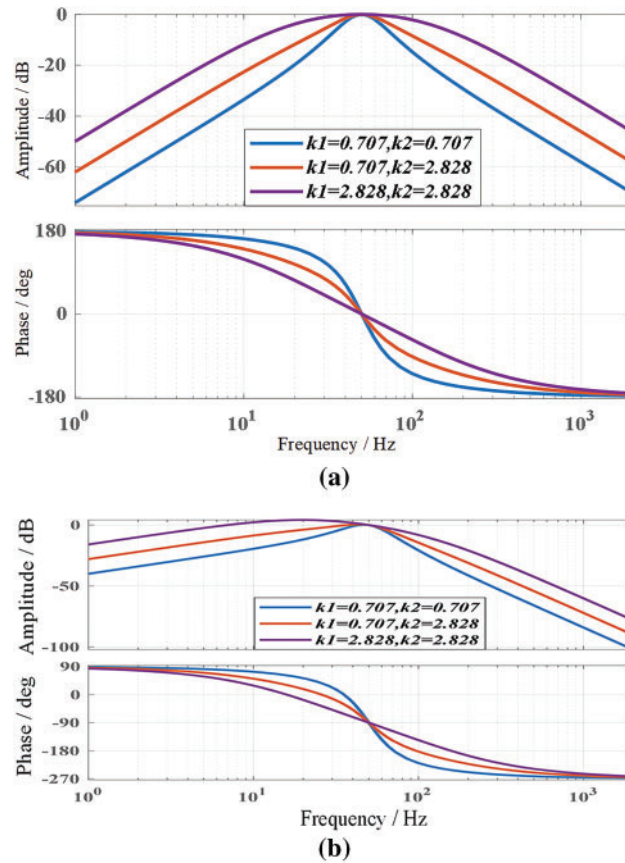


Figure 6: Bode plot of FCSOGI under different coefficients. (a) $D_{\text{FCSOGI}}(s)$ bode plot; (b) $Q_{\text{FCSOGI}}(s)$ bode plot

From Fig. 6, it can be seen that as k_1 and k_2 increase, the bandwidth of FCSOGI gradually increases, and the dynamic response speed becomes faster, but the filtering ability for harmonics weakens. Therefore, considering all aspects, this article selects $k_1 = 0.707$ and $k_2 = 2.828$.

Fig. 7 compares the Bode plots of the transfer functions of SOGI and FCSOGI under approximate dynamic response time. Among them, the dynamic response curve is shown in Fig. 8, with a time of about 30 ms. From Fig. 7, it can be seen that FCSOGI has stronger filtering ability at harmonics of various frequencies, and improves the suppression defect of the original $Q_{\text{SOGI}}(s)$ that cannot suppress DC signals. FCSOGI has a filtering ability of over 90% for harmonics of 5 or more. Compared with SOGI, FCSOGI keeping a good dynamic response time, and the filtering ability of each harmonic is improved, thereby better eliminating the impact of low-order harmonics on the accuracy of power grid signal synchronization detection.

Table 1 compares the distortion rates of signals v_α and v_β in the FCSOGI-PLL proposed in this paper with classical SRF-PLL [11] and SOGI-PLL [26] phase-locked loops injected with 5th, 7th, 11th, and 13th harmonics under frequency fluctuation conditions.

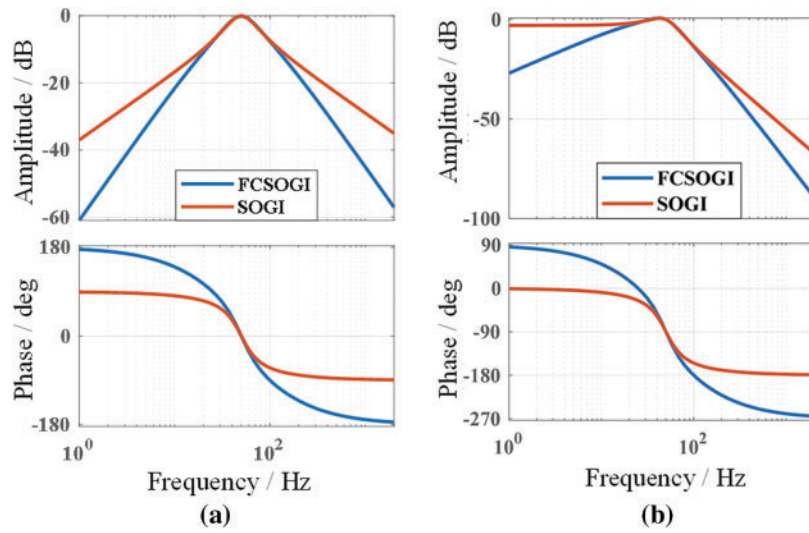


Figure 7: FCSOGI and SOGI Bode plots. (a) $D(s)$; (b) $Q(s)$

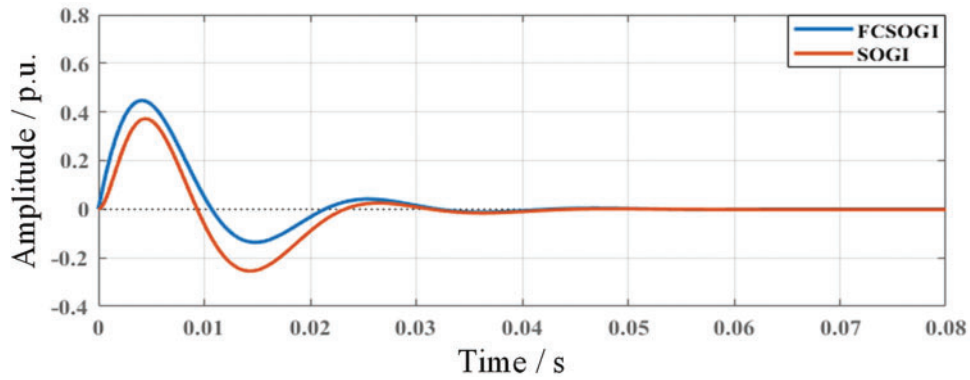


Figure 8: FCSOGI and SOGI step response diagram

Table 1: THD of input signals in different stages of PLL

	SRF-PLL	SOGI-PLL	FCSOGI-PLL
50 Hz harmonic condition	7.9%	1.06%	0.35%
55 Hz harmonic condition	7.86%	1%	0.3%
45 Hz harmonic condition	7.89%	1.14%	0.37%

From Table 1, it can be seen that the proposed FCSOGI-PLL method can ensure high-quality signals under different frequency conditions, thereby avoiding interference with the phase-locked loop, and the filtering ability is relatively stable. Meanwhile, using the SOGI-PLL method, the amplitude error of the output signal v_d under frequency fluctuation conditions is $\pm 1.5\%$, while the FCSOGI-PLL error proposed in this paper is only $\pm 0.4\%$. Therefore, the proposed FCSOGI-PLL method can better filter and output orthogonal signals, and ensure the accuracy of amplitude and phase angle detection under frequency fluctuations.

In order to eliminate the influence of the second harmonic component generated by the Park transformation of the unbalanced voltage component in the power grid on the two-phase signals of the phase-locked loop v_d and v_q . In the $\alpha\beta$ coordinate system, using the orthogonal signals v_α and v_β output by FCSOGI, the positive and negative sequence components can be obtained through a certain orthogonal transformation from the orthogonal components, and there is no zero sequence component, as shown in Eq. (20).

$$\begin{cases} v_{\alpha\beta}^+ = \frac{1}{2} \begin{bmatrix} 1 & -q \\ q & 1 \end{bmatrix} v_{\alpha\beta} \\ v_{\alpha\beta}^- = \frac{1}{2} \begin{bmatrix} 1 & q \\ -q & 1 \end{bmatrix} v_{\alpha\beta} \end{cases} \quad (20)$$

Based on the above analysis, the overall formed FCSOGI-PLL phase-locked loop is shown in Fig. 9. The phase-locked loop can first suppress the disturbance of DC components and complex harmonic components through a pre-filtering link, and at the same time compensate for orthogonal output based on the grid frequency. The extraction of positive and negative sequence components of unbalanced components can be achieved through the positive and negative sequence separation process. Finally, the real-time phase, frequency, and amplitude of the power grid are calculated using a phase-locked loop.

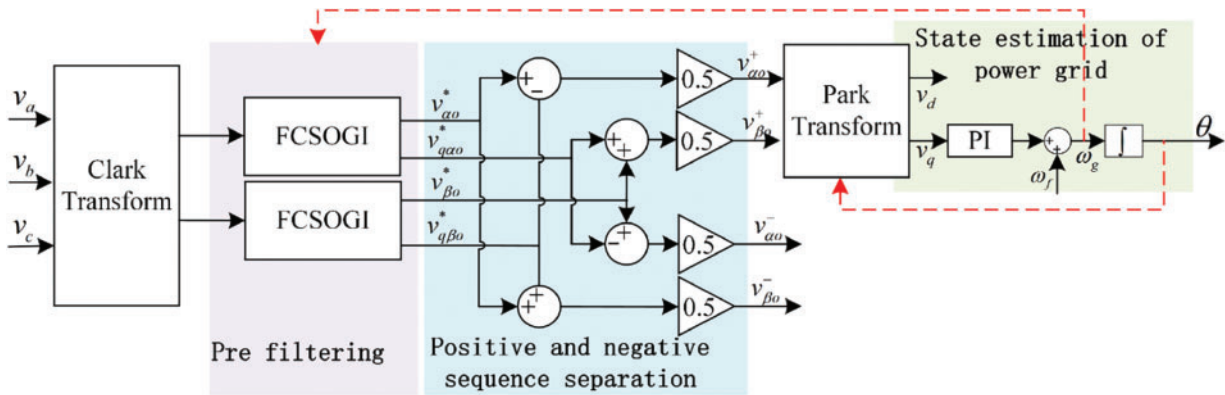


Figure 9: Structure of FCSOGI-PLL phase locked loop

4 Experimental Verification

In order to verify the effectiveness of the designed phase-locked loop structure, two experiments were conducted. Firstly, the FSOGI a frequency adaptive grid synchronization detection capability designed in Section 3.1 was validated under frequency fluctuation conditions to verify the rationality of the amplitude compensation branch designed. Secondly, verify the grid synchronization detection capability of the FCSOGI designed in Section 3.2 under complex grid conditions to validate the rationality of the designed series FSOGI structure. In the experiment, the main circuit of the three-phase power grid system was imported into the real-time simulator through the StarSim HIL software of the upper computer, and the phase-locked loop control structure was imported into the controller through the RCP software of the upper computer. The sampling frequency is 15 kHz, and the two are transmitted through wiring terminals. The experimental platform is shown in Fig. 10.

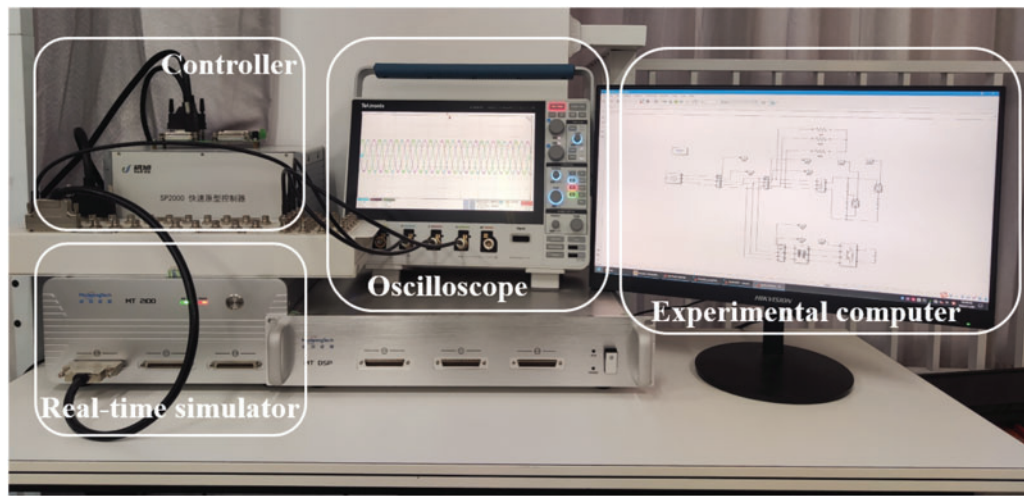


Figure 10: Experimental platform

Experiment 1: Design two power grid operating conditions, and compare the grid synchronization detection capabilities of FSOGI-PLL and SOGI-PLL phase-locked loops. The first condition is to increase the frequency by 5 Hz, while the second condition is to decrease the frequency by 5 Hz. Figs. 11–13 respectively show the actual power grid voltage waveform, the phase-locked loop detection frequency, the positive sequence voltage waveform detected by the phase-locked loop (phase A), and the detection of positive sequence voltage error.

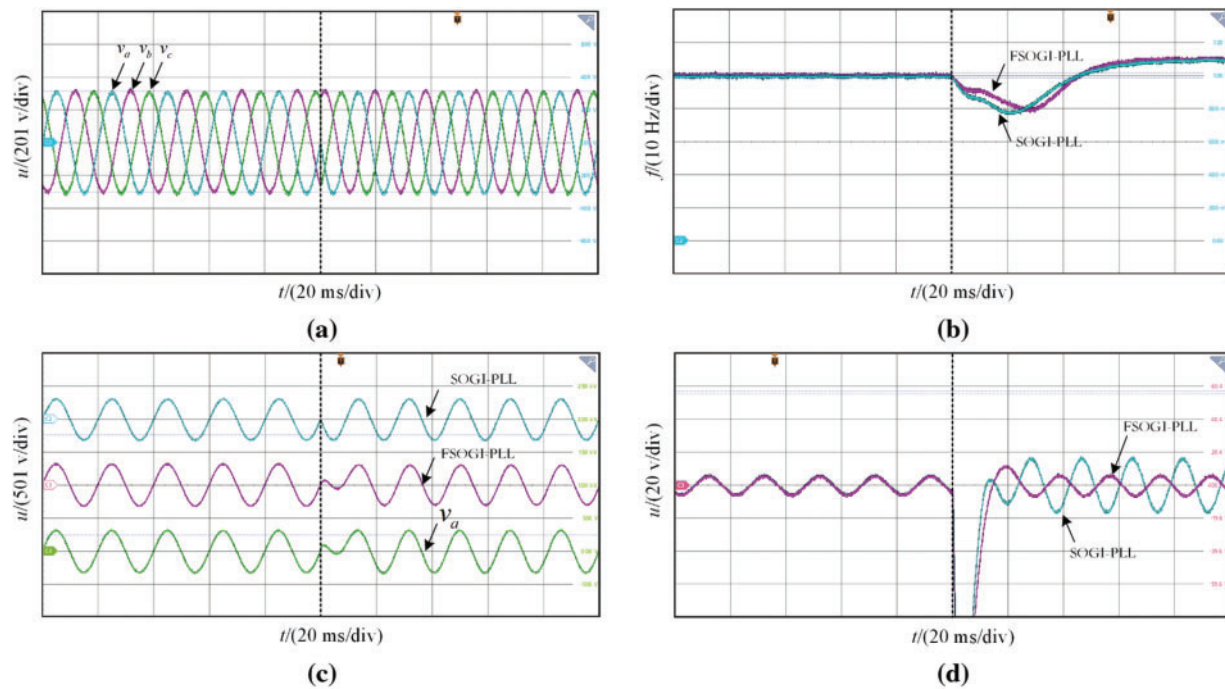


Figure 11: Condition one: Frequency increase by 5 Hz. (a) Grid voltage waveform; (b) PLL detection frequency; (c) Detection positive sequence; (d) Voltage detection error

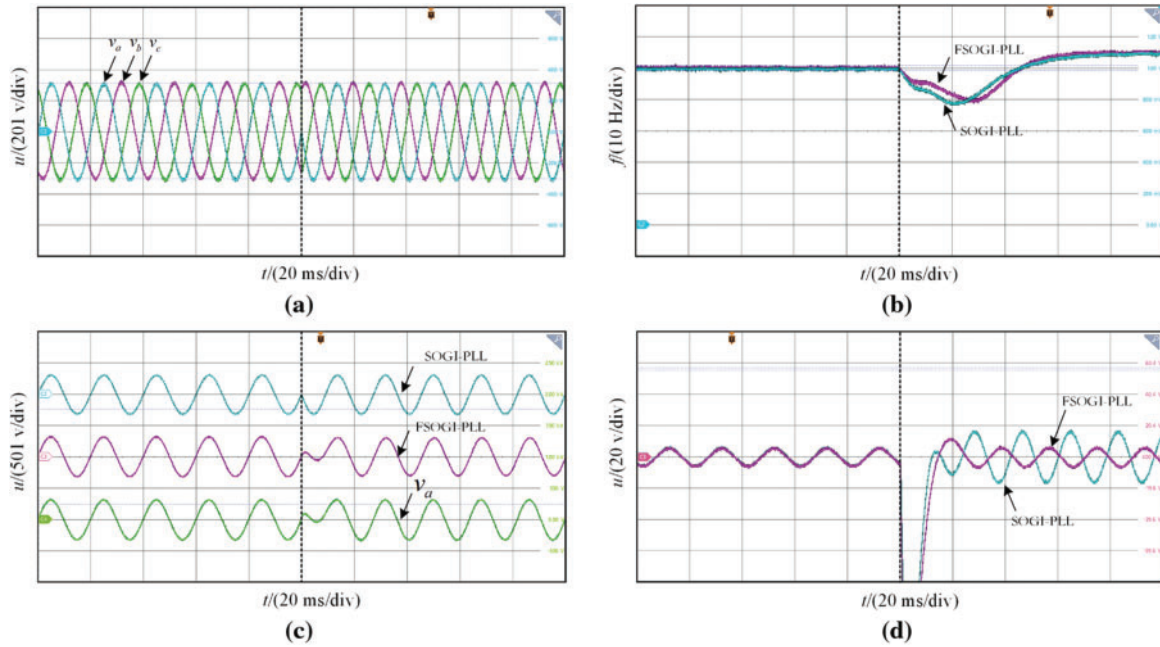


Figure 12: Condition two: Frequency decrease by 5 Hz. (a) Grid voltage waveform; (b) PLL detection frequency; (c) Detection positive sequence; (d) Voltage detection Error

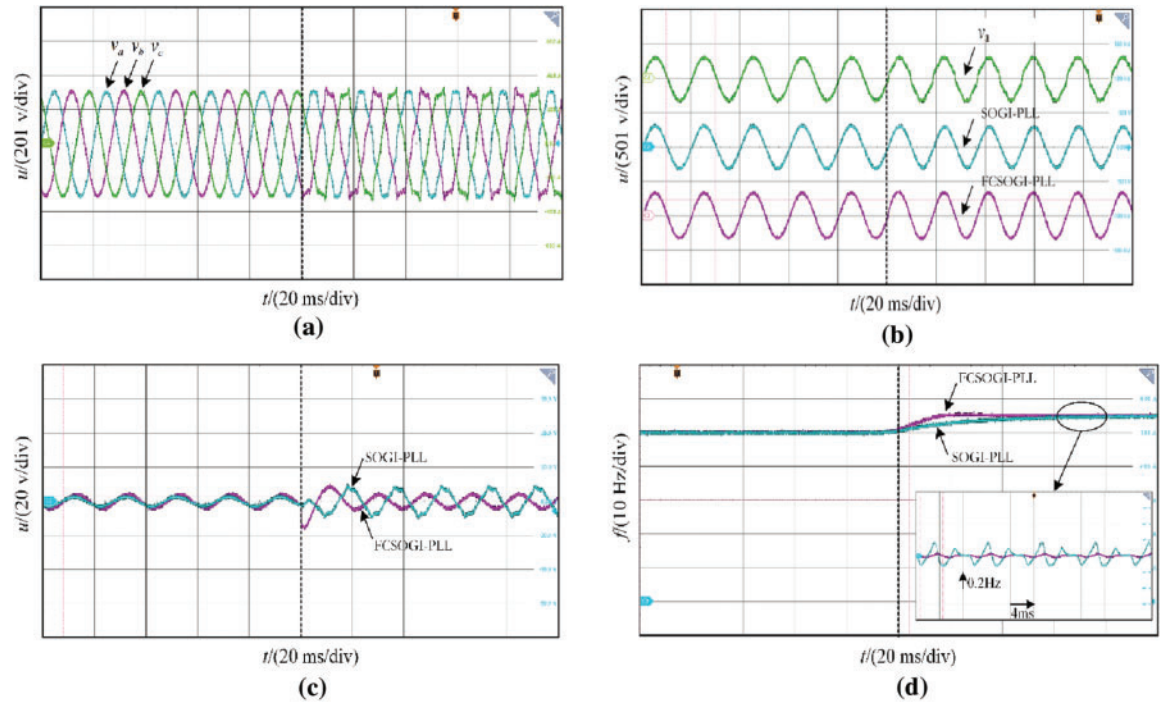


Figure 13: Grid synchronization detection condition one. (a) Grid voltage waveform; (b) Detection positive sequence; (c) Voltage detection error; (d) PLL detection frequency

From Figs. 11 and 12, it can be seen that under the conditions of increasing and decreasing frequency, FSOGI-PLL has a faster frequency detection speed compared to SOGI-PLL. This is mainly because the

designed amplitude compensation branch has frequency adaptive adjustment ability for the fundamental frequency signal, which can track the fluctuations of the power grid frequency faster. From Figs. 11c and 12c, both phase-locked loops can detect the positive sequence voltage of the power grid. From Figs. 11c and 12c, FSOGI has a smaller error in detecting the positive sequence voltage of the power grid, and there is almost no additional error under frequency fluctuations. This further verifies that the designed amplitude compensation branch applied to SOGI can achieve higher precision grid synchronization detection under frequency fluctuation conditions.

Experiment 2: Design three power grid operating conditions, and compare the grid synchronization detection capabilities of FCSOGI-PLL and SOGI-PLL phase-locked loops, to verify the accuracy of the designed phase-locked loop in synchronous detection of power grids under complex conditions of harmonics, frequency fluctuations, and three-phase imbalance. The experimental conditions for the three working conditions are as follows:

Condition one: Inject 5% of the 5th and 7th harmonics into the system under ideal grid conditions; 2.5% of the 11th and 13th harmonics, and 1.5% of the 17th and 19th harmonics, while increasing the frequency by 5 Hz.

Condition two: Inject the same harmonics as Scenario 1 into the system under ideal grid conditions, while reducing the frequency by 5 Hz.

Condition three: Under ideal grid conditions, inject the same harmonics as Scenario 1 into the system, while reducing the frequency by 5 Hz and lowering the A-phase voltage and C-phase voltage.

Figs. 13–15 show the voltage waveforms of the power grid under three different operating conditions, the fundamental positive sequence voltage detected by the phase-locked loop (taking phase A as an example), the voltage error diagram, and the output frequency diagram of the phase-locked loop.

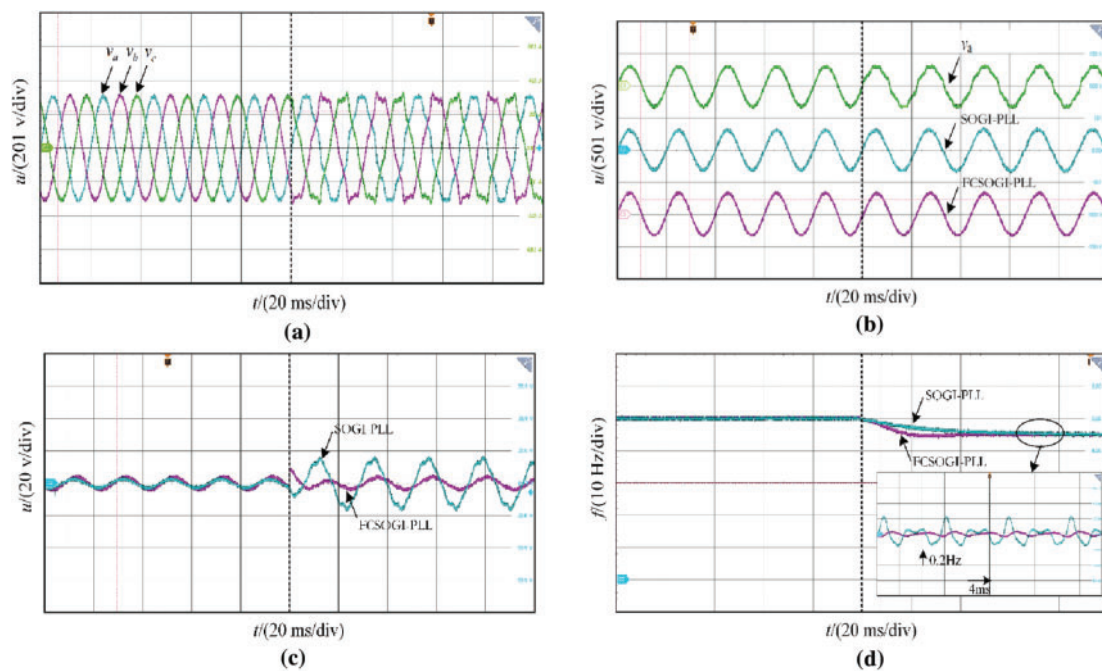


Figure 14: Grid synchronization detection condition two. (a) Grid voltage waveform; (b) Detection positive sequence; (c) Voltage detection error; (d) PLL detection frequency

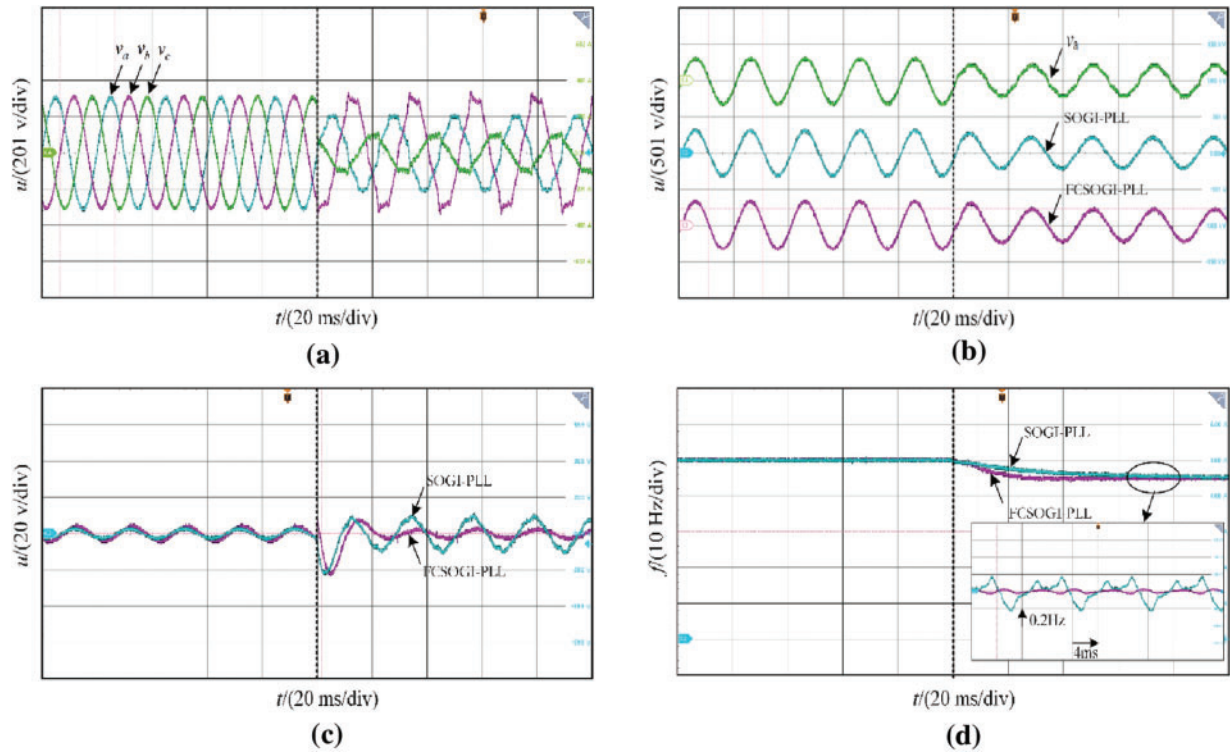


Figure 15: Grid synchronization detection condition three. (a) Grid voltage waveform; (b) Detection positive sequence; (c) Voltage detection error; (d) PLL detection frequency

Taking the A-phase voltage as an example, Figs. 13b, 14b, and 15b compare the actual voltage of the power grid with the positive sequence voltage detected by two types of phase-locked loops. It can be seen that the designed FCSOGI-PLL can better filter out harmonics in the power grid under different operating conditions, with a harmonic distortion rate maintained below 0.5%. The voltage distortion rate detected by the SOGI-PLL is around 1%, which verifies that the positive sequence fundamental frequency power grid voltage quality detected by the designed series structure is higher. Meanwhile, by introducing the positive and negative sequence separation modules, it can be seen that both phase-locked loops can stably detect the fundamental positive sequence voltage of the power grid under three-phase unbalanced conditions.

Figs. 13c, 14c, and 15c show the voltage errors detected under three operating conditions. It can be seen that due to frequency fluctuations, there is a significant error in tracking the fundamental frequency voltage of SOGI-PLL under fixed parameters, with voltage errors ranging from $\pm 3\%$ to $\pm 5\%$ at different frequencies. The designed FCSOGI-PLL has an amplitude compensation loop, which can ensure the detection accuracy of the fundamental frequency voltage at different frequencies. Under three different frequency variations, there is almost no additional error, and the voltage error is approximately the same as that under the original ideal power grid, and remains unchanged at $\pm 1.2\%$. This error is the inherent error of the filter. It also verifies that it has better frequency adaptation capability while ensuring the quality of the detected fundamental frequency positive sequence voltage.

It can be seen from the detection frequency in Figs. 13d, 14d and 15d, both phase-locked loops can track the changes in system frequency. The output frequency dynamic response of SOGI-PLL is slow due to the fixed parameters, and the output frequency error is ± 0.2 Hz due to the lack of filtering ability. Under different working conditions, FCSOGI-PLL can detect the power grid frequency stably in about 30 ms, and

the accuracy of frequency detection is greatly improved, with an error of only ± 0.02 Hz, which can meet the standard requirements of detection. It also verifies that the designed FCSOGI-PLL has better power grid synchronization detection capability.

5 Summary

In response to the problem of insufficient output accuracy of the original SOGI-PLL under complex power grid conditions, this paper designs an FCSOGI-PLL phase-locked loop structure. A feedforward amplitude compensation method was designed to compensate for the output orthogonal signal caused by frequency fluctuations, ensuring the accuracy of fundamental frequency voltage detection; In response to the insufficient filtering ability of SOGI, a two-stage series structure was designed to enhance the filtering ability and the suppression ability of DC components. The experimental results show that the FCSOGI-PLL designed for detecting the fundamental frequency positive sequence voltage of the power grid has higher quality, with a distortion rate of less than 0.5%, and the detected voltage error remains basically unchanged at different frequencies. The phase-locked loop detection system has higher frequency accuracy, with an error of only ± 0.02 Hz under different operating conditions, and can achieve tracking within 1.5 power frequency cycles. The output of this phase-locked loop can provide stable support for the power grid under complex operating conditions, further enhancing the stability and safety of the power system.

Acknowledgement: The authors received funding from the Science and Technology Project of China Southern Power Grid Co., Ltd., the National Key R&D Program of China, and the Innovation Capability Support Program of Shaanxi. We gratefully acknowledge these contributions.

Funding Statement: This research was supported by the Science and Technology Project of China Southern Power Grid Co., Ltd. (Grant No. ZBKJXM20232471), the National Key R&D Program of China (Grant No. 2021YFB1600200), the Innovation Capability Support Program of Shaanxi (Grant No. 2022KXJ-144).

Author Contributions: The authors confirm their contribution to the paper as follows: Conceptualization, Jie Shao and Zihao Zhang; Experiment, Quan Xu and Tiantian Cai; Writing—original draft preparation, Junye Li and Baicheng Xiang; Writing—review and editing, Shijie Li and Xianfeng Xu. All authors reviewed the results and approved the final version of the manuscript.

Availability of Data and Materials: Not applicable.

Ethics Approval: Not applicable.

Conflicts of Interest: The authors declare no conflicts of interest to report regarding the present study.

References

1. Rosso R, Wang X, Liserre M, Lu X, Engelken S. Grid-forming converters: control approaches, grid-synchronization, and future trends—a review. *IEEE Open J Ind Appl.* 2021;2:93–109. doi:10.1109/OJIA.2021.3074028.
2. Xiao H, He H, Zhang L, Liu T. Adaptive grid-synchronization based grid-forming control for voltage source converters. *IEEE Trans Power Syst.* 2024;39(2):4763–6. doi:10.1109/TPWRS.2023.3338967.
3. Lin X, Wen H, Yu J, Yu R. Adverse influence of PLL on the bus voltage feed-forward with band pass filter under harmonic and unbalance condition. *IEEE Trans Power Deliv.* 2021;36(2):1233–6. doi:10.1109/TPWRD.2020.3025465.
4. Lin X, Yu R, Yu J, Wen H. Constant-coupling-effect-based PLL for synchronization stability enhancement of grid-connected converter under weak grids. *IEEE Trans Ind Electron.* 2023;70(11):11310–23. doi:10.1109/TIE.2022.3227268.

5. Silwal S, Karimi-Ghartemani M, Karimi H, Davari M, Zadeh SMH. A multivariable controller in synchronous frame integrating phase-locked loop to enhance performance of three-phase grid-connected inverters in weak grids. *IEEE Trans Power Electron.* 2022;37(9):10348–59. doi:10.1109/TPEL.2022.3164878.
6. Eskandari M, Savkin AV. Robust PLL synchronization unit for grid-feeding converters in micro/weak grids. *IEEE Trans Ind Inform.* 2023;19(4):5400–11. doi:10.1109/TII.2022.3180074.
7. Golestan S, Guerrero JM, Vasquez JC. A PLL-based controller for three-phase grid-connected power converters. *IEEE Trans Power Electron.* 2018;33(2):911–6. doi:10.1109/TPEL.2017.2719285.
8. Kanjiya P, Khadkikar V, El Moursi MS. Obtaining performance of type-3 phase-locked loop without compromising the benefits of type-2 control system. *IEEE Trans Power Electron.* 2018;33(2):1788–96. doi:10.1109/TPEL.2017.2686440.
9. Vasudevan N, Venkatraman V, Ramkumar A, Muthukumar T, Sheela A, Vetrivel M, et al. Design and development of an intelligent energy management system for a smart grid to enhance the power quality. *Energy Eng.* 2023;120(8):1747–61. doi:10.32604/ee.2023.027821.
10. Zhang B, Jin Y. Grid-connected control strategy of VSG under complex grid voltage conditions. *Energy Eng.* 2022;119(4):1467–82. doi:10.32604/ee.2022.018233.
11. Verma AK, Jarial RK, Rao UM, Roncero-Sánchez P. A robust three-phase prefiltered phase locked-loop for the subcycle estimation of fundamental parameters. *IEEE Trans Ind Appl.* 2021;57(6):6155–66. doi:10.1109/TIA.2021.3105615.
12. Gude S, Chu CC, Vedula SV. Recursive implementation of multiple delayed signal cancellation operators and their applications in prefiltered and in-loop filtered PLLs under adverse grid conditions. *IEEE Trans Ind Appl.* 2019;55(5):5383–94. doi:10.1109/TIA.2019.2927190.
13. Singh JK, Prakash S, Behera RK. A nonlinear loop filter based PLL with harmonic filtering capability for single-phase grid integrated system with improved dynamic performance. *IEEE Trans Power Deliv.* 2022;37(6):4869–79. doi:10.1109/TPWRD.2022.3162071.
14. García JI, Candela JI, Catalán P. Prefiltered synchronization structure for grid-connected power converters to reduce the stability impact of PLL dynamics. *IEEE J Emerg Sel Top Power Electron.* 2021;9(5):5499–507. doi:10.1109/JESTPE.2020.3026916.
15. Li J, Wang Q, Xiao L, Hu Y, Wu Q, Liu Z. An $\alpha\beta$ -frame moving average filter to improve the dynamic performance of phase-locked loop. *IEEE Access.* 2020;8:180661–71. doi:10.1109/ACCESS.2020.3028237.
16. Taheri P, Amini J, Moallem M. Variable window size moving average filter for phase-locked-loop synchronization. *IEEE Access.* 2024;12:88111–21. doi:10.1109/ACCESS.2024.3417179.
17. Sevilmiş F, Karaca H, Ahmed H. High-order delayed signal cancellation-based PLL under harmonically distorted grid voltages. *IEEE Trans Instrum Meas.* 2023;72:9003609. doi:10.1109/TIM.2023.3298411.
18. Golestan S, Guerrero JM, Vasquez JC, Abusorrah AM, Al-Turki Y. Advanced single-phase DSC-based PLLs. *IEEE Trans Power Electron.* 2019;34(4):3226–38. doi:10.1109/TPEL.2018.2856931.
19. da Silva MJ, Ferreira SC, da Silva JP, dos Santos MG, Paganotti AL, Barbosa LM. Equivalency between adaptive Notch filter PLL and inverse park PLL by modeling and parameter adjustment. *IEEE Lat Am Trans.* 2020;18(12):2112–21. doi:10.1109/TLA.2020.9400439.
20. Gautam S, Xiao W, Ahmed H, Lu DD. Enhanced single-phase phase locked loop based on complex-coefficient filter. *IEEE Trans Instrum Meas.* 2022;71:9001408. doi:10.1109/TIM.2022.3147891.
21. Du X, Liu Y, Wang G, Sun P, Tai HM, Zhou L. Three-phase grid voltage synchronization using sinusoidal amplitude integrator in synchronous reference frame. *Int J Electr Power Energy Syst.* 2015;64(5):861–72. doi:10.1016/j.ijepes.2014.08.005.
22. Prakash S, Singh JK, Behera RK, Mondal A. A type-3 modified SOGI-PLL with grid disturbance rejection capability for single-phase grid-tied converters. *IEEE Trans Ind Appl.* 2021;57(4):4242–52. doi:10.1109/TIA.2021.3079122.
23. Ahmed H. Low-order measurement offset rejection methods in single-phase SOGI-PLL. *IEEE Sens Lett.* 2024;8(1):7000604. doi:10.1109/LSSENS.2023.3347676.

24. Xian X, Wen M, Yong L, Yang Y, Zhen Z. Frequency adaptive active power filtering control strategy based on harmonic characteristics of a charging station. *Power Syst Prot Control*. 2024;52(21):24–34. doi:10.19783/j.cnki.pspc.240488.
25. Mellouli M, Hamouda M, Ben Hadj Slama J, Al-Haddad K. A third-order MAF based QT1-PLL that is robust against harmonically distorted grid voltage with frequency deviation. *IEEE Trans Energy Convers*. 2021;36(3):1600–13. doi:10.1109/TEC.2021.3061027.
26. Mohamadian S, Pairo H, Ghasemian A. A straightforward quadrature signal generator for single-phase SOGI-PLL with low susceptibility to grid harmonics. *IEEE Trans Ind Electron*. 2022;69(7):6997–7007. doi:10.1109/TIE.2021.3095813.